

1 **Contributions of Surface Solar Radiation and Precipitation to the Spatiotemporal**  
2 **Patterns of Surface and Air Temperature Warming in China from 1960 to 2003**

3 Jizeng Du<sup>1,2</sup>, Kaicun Wang<sup>1,2\*</sup>, Jiankai Wang<sup>3</sup>, Qian Ma<sup>1,2</sup>

4 <sup>1</sup>College of Global Change and Earth System Science, Beijing Normal University,  
5 Beijing, 100875, China

6 <sup>2</sup>Joint Center for Global Change Studies, Beijing 100875, China

7 <sup>3</sup>Chinese Meteorological Administration, Beijing, 100081, China

8 **Corresponding author:** Kaicun Wang, College of Global Change and Earth System  
9 Science, Beijing Normal University. Email: [kcwang@bnu.edu.cn](mailto:kcwang@bnu.edu.cn); Tel: +086 10-  
10 58803143; Fax: +086 10-58800059.

11

12 **Submitted to Atmospheric Chemistry and Physics**

13 **February 18, 2016**

14

15 **Abstract**

16 **Although global warming has been attributed to increases in atmospheric**  
17 **greenhouses gases, the mechanisms underlying spatiotemporal patterns of**  
18 **warming trends remain under debate. Herein, we analyzed surface and air**  
19 **warming observations recorded at 1,977 stations in China from 1960 to 2003. Our**  
20 **results showed a significant spatial pattern for the warming of the daily maximum**  
21 **surface ( $T_{s-max}$ ) and air ( $T_{a-max}$ ) temperatures, and the pattern was stronger in**  
22 **northwest China and weaker in South China and the North China Plain. These**  
23 **warming spatial patterns were attributed to surface shortwave solar radiation ( $R_s$ )**  
24 **and precipitation ( $P$ ), which represent the key parameters of the surface energy**  
25 **budget. During the study period,  $R_s$  decreased by  $-1.50\pm 0.42 \text{ W m}^{-2} 10\text{yr}^{-1}$  in**  
26 **China, which caused the trends in  $T_{s-max}$  and  $T_{a-max}$  to decrease by 0.139 and**  
27 **0.053 °C  $10\text{yr}^{-1}$ , respectively. More importantly, the decreasing rates in South**  
28 **China and the North China Plain were much higher than those in other regions.**  
29 **The spatial contrasts in the trends of  $T_{s-max}$  and  $T_{a-max}$  in China were significantly**  
30 **reduced after adjusting for the effect of  $R_s$  and  $P$ . For example, after adjusting for**  
31 **the effect of  $R_s$  and  $P$ , the difference in the  $T_{s-max}$  and  $T_{a-max}$  values between the**  
32 **North China Plain and the Loess Plateau was reduced by 97.8% and 68.3%,**  
33 **respectively, the seasonal contrast in  $T_{s-max}$  and  $T_{a-max}$  decreased by 45.0% and**

34 **17.2%, respectively, and the daily contrast in the warming rates of the surface and**  
35 **air temperature decreased by 33.0% and 29.1%, respectively. This study showed**  
36 **that the land energy budget plays an essential role in the identification of regional**  
37 **warming patterns.**

## 38 **1. Introduction**

39       Increases in observational data and rapid developments in simulation capacity of  
40 climate models have provided evidence for the phenomenon of global warming  
41 (Hartmann et al., 2013), and the increases in anthropogenic greenhouse gases and other  
42 anthropogenic effects are considered the primary causes. However, significant spatial  
43 and temporal heterogeneities in climate warming have been observed. For example,  
44 faster warming rates occur in semiarid regions and a “warming hole” has been identified  
45 in the central United States (Boyles and Raman, 2003; Huang et al., 2012). These  
46 spatiotemporal heterogeneities represent a major barrier to the reliable detection and  
47 attribution of global warming (Tebaldi et al., 2005; Mahlstein and Knutti, 2010).  
48 Furthermore, uncertainties in model simulations generally increase from global to  
49 regional scales because of uncertainty in regional climatic responses to global change  
50 (Hingray et al., 2007; Mariotti et al., 2011). Therefore, investigations of the spatial and  
51 temporal patterns of regional climate changes and regional climatic response

52 mechanisms to global change are crucial for increasing the accuracy of models designed  
53 to detect and explain the causes of global climate change and predictions of future  
54 regional climate change.

55       The spatial heterogeneity of climate warming can be attributed to local climate  
56 factors and anthropogenic factors (Karl et al., 1991). For the local climate factors,  
57 determining factors such as cloud cover and precipitation ( $P$ ) can significantly influence  
58 the speed of regional warming (Hegerl and Zwiers, 2007; Lauritsen and Rogers, 2012).  
59 Spatial heterogeneities in climate-factor trends have an important influence on various  
60 changes in the land-surface energy balance. Studies have demonstrated that an increase  
61 in cloud cover can diminishes the surface solar radiation ( $R_s$ ) and therefore reduces the  
62 daytime temperature (Dai et al., 1997; Zhou et al., 2010; Taylor et al., 2011), although  
63 it has the potential to increase night-time temperature by intercepting outgoing  
64 longwave radiation (Shen et al., 2014; Campbell and VonderHaar, 1997).

65       Precipitation ( $P$ ) can alter the proportion of surface absorbed energy partitioned  
66 into sensible heat flux and latent heat flux; therefore it has an inevitable effect on both  
67 land-surface and near-surface air temperatures (Wang and Dickinson, 2012; Wang and  
68 Zhou, 2015). Additionally,  $P$  has a significant effect on soil thermal inertia and the  
69 response of surface vegetation, which results in an important feedback for regional and

70 global warming (Wang and Dickinson, 2012; Seneviratne et al., 2010; Ait-Mesbah et  
71 al., 2015; Shen et al., 2015).

72 In addition to local climate factors, regional climate systems are significantly  
73 affected by the anthropogenic emissions of aerosols. Studies have indicated that  
74 improvements in air quality in recent decades over North America and Europe have led  
75 to brightening effect (Wild, 2012; Vautard et al., 2009), whereas East Asia and India  
76 have led to declines in  $R_s$  (Xia, 2010; Menon et al., 2002; Wang et al., 2012; Wang et  
77 al., 2015a). Consequently, variations in  $R_s$  may have an effect on both local and global  
78 climate change (Wild et al., 2007; Wang and Dickinson, 2013b).

79 Changes in land cover can also alter the energy exchange between the land surface  
80 and the atmosphere, and such changes have the potential to affect regional climates  
81 (Falge et al., 2005; Bounoua et al., 1999; Zhou et al., 2004). Previous studies have  
82 suggested that urbanization and other land-use changes contribute to promoting the  
83 warming effect caused by greenhouse gases (Kalnay and Cai, 2003; Lim et al., 2005;  
84 Chen et al., 2015). Overall, the effects of these factors on climate change may be very  
85 important at the regional scale and could lead to marked spatial differences in regional  
86 climate change; however, they are usually omitted from the detection and attribution of  
87 climate change at the global scale (Karoly and Stott, 2006).

88 China is a vast territory that has an abundance of climactic zones stretching from  
89 tropical to cold temperate, and a special alpine climate is observed over the Tibet  
90 Plateau. Additionally, the dramatic economic development and explosive population  
91 growth in China in recent decades have caused significant changes in land cover and  
92 sever air pollution, including frequent haze events (Yin et al., 2016; Cheng et al., 2014;  
93 Wang et al., 2016). The climatic diversity and intensive human activity in this region  
94 will likely lead to a unique response to global warming with obvious spatial differences  
95 in climate change.

96 Karl et al. (1991) analyzed the observational records for the period 1951-1989 and  
97 found that warming trends in China were faster than those of the United States but  
98 slower than those of the former Soviet Union. Several studies have revealed that the  
99 warming rate in Northwest China was approximately 0.33-0.39 °C 10yr<sup>-1</sup> during the  
100 second half of the last century (Li et al., 2012; Zhang et al., 2010), which was  
101 significantly higher than the average warming rate over China of 0.25 °C 10yr<sup>-1</sup> (Ren  
102 et al., 2005) or the average global rate of 0.13 °C 10yr<sup>-1</sup> (Hegerl and Zwiers, 2007).  
103 The air temperature ( $T_a$ ) over the Tibet Plateau has increased by 0.44 °C 10yr<sup>-1</sup> over  
104 the last 30 years (Duan and Xiao, 2015), and this rate is considerably faster than the  
105 overall warming rate in the Northern Hemisphere (0.23 °C 10yr<sup>-1</sup>) and worldwide  
106 (0.16 °C 10yr<sup>-1</sup>) (Hartmann et al., 2013). To provide insights on global warming and

107 improve the accuracy of future climate change predictions, understanding the  
108 characteristics and mechanisms of regional climate change is critical.

109  $T_a$  is a common metric for determining climate change on the global or regional  
110 scales. The land surface temperature ( $T_s$ ) is also important in climate change research  
111 because of its direct relationship with the land surface energy budget. Previously,  $T_s$   
112 values used in regional climate research are primarily derived from satellite retrievals  
113 or reanalysis datasets (Weng et al., 2004; Peng et al., 2014), which both have  
114 satisfactory global coverage but questionable accuracy and integrity. Furthermore,  
115 satellite-derived  $T_s$  values are only available under clear sky conditions, thus limiting  
116 their applicability in climate change studies.

117 In China, both  $T_s$  and  $T_a$  are measured as conventional meteorological observation  
118 parameters by nearly all weather stations. An analysis of the spatiotemporal patterns of  
119 these parameters identified a close relationship between  $T_s$  and  $T_a$ , which indicates that  
120  $T_s$  and  $T_a$  present equivalent accuracy when used to determine the characteristics of  
121 climate change. More importantly,  $T_s$  is more sensitive than  $T_a$  to the local land surface  
122 energy budget.

123 Both  $R_s$  and  $P$  are key factors controlling the land surface energy budget; therefore,  
124 changes in these two factors most likely cause regional differences in the warming rate

125 of  $T_a$  (Wild, 2012; Manara et al., 2015; Hartmann et al., 1986). To our knowledge, this  
126 study presents the first analysis of the relationship between  $R_s$  (and  $P$ ) and  $T_a/T_s$  based  
127 on their spatiotemporal patterns and we further quantified the effect of variations of  $R_s$   
128 and  $P$  on  $T_a/T_s$  in China for the period 1960-2003.

129 This article is organized as follows. Section 2 introduces the data and methods  
130 used in the study. Section 3 describes the spatial and temporal patterns of climate  
131 warming over China, analyses the effect of the variation in  $R_s$  and  $P$  on  $T_a/T_s$ , and  
132 examines the spatial and temporal patterns of the warming trend of  $T_a/T_s$  after adjusting  
133 for the effects of  $R_s$  and  $P$ , which eliminated the effects of  $R_s$  and  $P$  on warming and  
134 highlighted the effects of large-scale warming caused by elevated concentrations of  
135 atmospheric greenhouse gases. Moreover, the spatial contrast in the warming trends of  
136  $T_a/T_s$  in China was substantially reduced after adjusting for the effect of  $R_s$  and  $P$ , and  
137 this result is consistent with the expectations under global warming. Finally, Section 4  
138 presents a summary and discussion.

## 139 **2. Data and methods**

### 140 **2.1. Data**

141 The meteorological observational data used in this study are included recently

142 released daily meteorological datasets, such as the China National Stations'  
143 Fundamental Elements Datasets V3.0 (CNSFED V3.0), and they were downloaded  
144 from China's National Meteorological Information Centre (<http://data.cma.gov.cn/data>)  
145 (Cao et al., 2016). These datasets included observations of  $T_s$ ,  $T_a$ , barometric pressure,  
146 relative humidity, and sunshine duration. All of the observational records of the climate  
147 variables were subjected to quality control measures, and the data acquisition and  
148 compilation.

149 As shown in Figure 1, the number of stations used in this study (1,977 stations  
150 selected from a total of 2,479 stations) was significantly higher than that of previous  
151 studies (i.e., 57-852 stations) (Kukla and Karl, 1993; Shen and Varis, 2001; Liu et al.,  
152 2004; Li et al., 2015). Therefore, the observational data provided better spatial coverage  
153 and higher confidence in the detection of regional climate change than in previous  
154 studies (Fig. 1). Our study is the first to use  $T_s$  observation as a parameter for identifying  
155 regional climate change.

156 Observations of  $T_s$  from weather stations are different from  $T_s$  data retrieved via  
157 other approaches, such as satellite images and reanalysis. The  $T_s$  observations were  
158 performed in  $4 \times 2$  m square bare land plots proximal to the weather stations. The  
159 surface of the observational fields was loose, grassless and flat, and at the same level

160 as the ground surface of the weather station. Three thermometers, including a surface  
161 thermometer, a surface maximum thermometer, and a surface minimum thermometer  
162 were placed horizontal to the surface of the observational field, with half of each  
163 thermometer embedded in the soil and the other half exposed to the air. When the  
164 observational field was covered by snow, the thermometers were placed on the snow  
165 surface. Additionally, the exposed parts of the thermometers were cleaned to remove  
166 dust and dew.

167 We verified the reliability of the  $T_s$  observational records by analyzing the  
168 relationship between  $T_a$  and  $T_s$  during 1960-2003. As shown in Figure. S1, the mean  
169 Pearson Correlation Coefficients between daily maximum land surface temperature ( $T_{s-}$   
170  $_{max}$ ) and daily maximum air temperature ( $T_{a-max}$ ) calculated from the monthly anomalies  
171 were 0.775, 0.843, and 0.806 for the annual, warm, and cold seasonal scales,  
172 respectively, and these values were statistically significant (99% confidence level) for  
173 all stations. The mean correlation coefficients between the daily minimum land surface  
174 temperature ( $T_{s-min}$ ) and daily minimum air temperature ( $T_{a-min}$ ) were 0.861, 0.842, and  
175 0.865 for the annual, warm, and cold seasonal scales, respectively, and these values  
176 were statistically significant (99% confidence level) for all stations. The high  
177 correlations indicated that observations of either  $T_s$  or  $T_a$  could be used for climate  
178 change detection.

179           The most fundamental energy resource for  $T_s$  and  $T_a$  is  $R_s$ . In most previous studies,  
180 the observed  $R_s$  have been used to analyze the relation between the variation in  $R_s$  and  
181  $T_a$  over China. However, fewer sites were used for  $R_s$  observations than for other  
182 climatic variables; for example, only 85 sites were used for  $R_s$  observations in Liu et al.  
183 (2004) and only 90 sites were used in Li et al. (2015).

184           Importantly, sensitivity drift the instruments used for the  $R_s$  observations led to a  
185 faster dimming rate before 1990, and instrument replacements from 1990 to 1993  
186 resulted in a false sharp increase in  $R_s$  (Wang, 2014; Wang et al., 2015a). The limited  
187 distribution and low quality of  $R_s$  observations have impeded the wide scientific  
188 application of this parameter.

189           Therefore, we used sunshine duration-derived  $R_s$ , which is based on an effective  
190 hybrid model developed by Yang et al. (2006). This model has subsequently been  
191 improved (Wang et al., 2015a; Wang, 2014) and it has performed well in regional and  
192 global applications (Tang et al., 2011; Wang et al., 2012). Sunshine duration-derived  $R_s$   
193 not only accurately reflects the effects of clouds and aerosols on the  $R_s$  but also more  
194 exactly reveals long-term trends (Wang et al., 2015a; Wang, 2014). Additionally,  
195 sunshine duration-derived  $R_s$  values are better correlated with the satellite retrievals,  
196 reanalyzes, and climate model simulations than  $R_s$  values observed from observation

197 (Wang et al., 2015a).

198 The data are collected by a total of 2,474 meteorological stations; however, the  
199 lengths of the effective observation records for the stations are different. Additionally,  
200 only a small number of stations were installed before 1960, and the observational  
201 records of  $T_s$  at many stations were anomalous after 2003 because of automation.  
202 Therefore, in our analysis, we selected 1,977 meteorological stations (see Fig 1) for  
203 which the observation records with valid data were longer than 30 years during the 43  
204 years between 1960 and 2003.

205 The monthly anomalies relative to the 1961-1990 climatology were calculated  
206 based on a monthly mean value of the daily values, and when a month was missing  
207 more than 7 daily values, that month was classified as a missing value (Sun et al., 2016;  
208 Li et al., 2015). For the annual anomalies, the monthly anomalies were averaged for the  
209 entire year. The anomalies in the warm seasons were the averages of the monthly  
210 anomalies from May to October, and the anomalies in the cold seasons were the  
211 averages of the monthly anomalies from November to the next April.

## 212 **2.2 Methods**

213 As shown in Fig 1, the spatial distribution of the weather stations throughout China

214 is extraordinarily asymmetric and the density of weather stations in east China is far  
215 greater than that in west China. We used the area-weight average method to reduce these  
216 biases when calculating the national mean. First, we divided the study region into  $1^\circ \times$   
217  $1^\circ$  grids (see Fig S2) for a total 953 grids covering China. Second, we assigned all  
218 selected stations to the grids, and this resulted in 627 grids containing stations, which  
219 accounted for 65.79% of the total. Finally, the grid box value was the average of all  
220 stations in the grid, and the national mean was the area-weight average of all effective  
221 grids (Jones and Moberg, 2003).

222 The linear trends reported in this study were calculated via linear regression based  
223 on the monthly anomalies of  $T$ ,  $R_s$ , and  $P$ . Two national mean trends were calculated  
224 from the anomalies of the grids. In the first method (Method I), the national mean  
225 monthly anomalies were calculated using the area-weight of each grid first, and then  
226 the national mean trend based on the time series of the national average anomalies was  
227 calculated. In the second method (Method II), the trend at each grid was calculated first,  
228 and then the national mean trend was calculated from the grid trends.

229 In our study, we calculated the national mean trends of the temperatures using  
230 Method I and II because both methods have been used in previous studies (Gettelman  
231 and Fu, 2008). The results for the two methods are expected to be the same when the

232 time series of all grids is integrated and data are not missing (Zhou et al., 2009);  
233 however, when data are missing, small differences may occur (See Table 1). As shown  
234 in Table 1, the absolute value of the difference between Method I and Method II ranged  
235 from 0.011 to 0.033 °C 10yr<sup>-1</sup>, which represented 3.4% to 14.3% of the trends (using  
236 the results of Method I as the reference). For purposes of clarification, the trends  
237 derived from Method I are discussed in the main text, whereas the results from both  
238 methods are shown in Table 1.

239 The effect of  $R_s/P$  on  $T_{s-max}/T_{a-max}$  was determined via a multiple linear regression  
240 (Roy and Haigh, 2011) of the monthly anomalies using the following equation:

$$241 \quad T = S_{R_s} \cdot R_s + S_P \cdot P + c + \varepsilon \quad (1)$$

242 where  $T$  represents the monthly anomalies of  $T_{s-max}$ ,  $T_{s-min}$ ,  $T_{a-max}$ , and  $T_{a-min}$ ;  $S_{R_s}$  and  $S_P$   
243 are the sensitivities of the temperatures to  $R_s$  and  $P$ , respectively;  $c$  is constant term;  
244 and  $\varepsilon$  indicates the residuals of the equation. The coefficients of determination ( $R^2$ )  
245 for the multilinear regression equation (Eq (1)) are shown in Fig S3, and they indicate  
246 the portion of the variance of  $T$  that could be attributed to that of  $R_s$  and  $P$ . High  
247 coefficients of determination were obtained, which showed that the linear regression  
248 performed well, particularly for South China and the North China Plain. To separate the  
249 contributions of  $R_s$  and  $P$ , we further calculated the partial correlation coefficients

250 between  $R_s$  and  $T$  (or  $P$  and  $T$ ), which are shown in Fig S4 and Fig S5.

251 To determine the effect of  $R_s/P$  on the analyzed temperatures, we removed their  
252 effects from their original time series of  $T_{s-max}$  and  $T_{a-max}$  based on the multilinear  
253 relationship calculated in Eq (1). Then, we calculated the trends from both the original  
254 and adjusted time series. By comparing the derived trends of the original and adjusted  
255 time series, we quantitatively assessed the effect of  $R_s/P$  on  $T_{s-max}$  and  $T_{a-max}$ , particularly  
256 for the spatiotemporal pattern of their trends.

### 257 **3. Results**

#### 258 **3.1. Trends of surface temperature and air temperature**

##### 259 **3.1.1 Temporal patterns in temperature variability**

260 The long-term changes in  $T_{s-max}$  and  $T_{a-max}$  and  $T_{s-min}$  and  $T_{a-min}$  from 1960 to 2003  
261 are shown in Fig 2 and Fig 3, respectively. In addition to the annual variability (Fig 2a  
262 and Fig 3a), the temperature variability in both warm seasons (May-October; Fig 2b  
263 and Fig 3b) and cold seasons (November to the following April; Fig 2c and Fig 3c)  
264 were analyzed. In the annual records, all temperatures exhibited an obvious warming  
265 trend throughout China (Fig 2a and Fig 3a).

266 As shown in Table 1, the national mean warming rate from 1960 to 2003 for  $T_{s-max}$   
267 was  $0.227 \pm 0.091$  °C  $10yr^{-1}$  (95% confidence level) and  $T_{a-max}$  was  $0.167 \pm 0.068$  °C  
268  $10yr^{-1}$  (95% confidence level). The warming rate of  $T_{a-max}$  based on the 1,977 stations  
269 examined in the current study was slightly higher than the global average ( $0.141$  °C  
270  $10yr^{-1}$ ) from 1950 to 2004 (Vose et al., 2005) and the rate obtained from a previous  
271 analysis ( $0.127$  °C  $10yr^{-1}$ ) of temperatures from 1955 to 2000 based on 305 stations in  
272 China (Liu et al., 2004). Additionally, the increases in  $T_{s-max}$  and  $T_{a-max}$  in the cold  
273 seasons were much larger than those in the warm seasons, which is consistent with  
274 previous studies of China and other regions (Shen et al., 2014; Vose et al., 2005; Ren et  
275 al., 2005).

276 Similarly, the warming rates of  $T_{s-min}$  and  $T_{a-min}$  in the warm seasons were also  
277 clearly lower than those in the cold seasons. As shown in Fig 3,  $T_{s-min}$  increased by  
278  $0.315 \pm 0.058$  °C  $10yr^{-1}$  (95% confidence level) and  $T_{a-min}$  increased by  $0.356 \pm 0.0057$  °C  
279  $10yr^{-1}$  (95% confidence level) (see Fig 3a) from 1960 to 2003. The warming trend of  
280  $T_a$  is generally consistent with earlier studies (Shen et al., 2014; Li et al., 2015; Liu et  
281 al., 2004); however, these trends are considerably larger than the rates reported for the  
282 global average ( $0.204$  °C  $10yr^{-1}$ ) (Vose et al., 2005). For the seasonal scales, the  
283 warming rate of  $T_{s-min}/T_{a-min}$  in the cold seasons was almost double that of the warm  
284 seasons from 1960 to 2003 (see Table 1).

285 The warming rate of  $T_{s-min}$  ( $T_{a-min}$ ) was significantly faster than that of  $T_{s-max}$  ( $T_{a-$   
286  $max$ ) and the warming rates of all temperatures in the cold seasons were substantially  
287 greater than those in the warm seasons (Li et al., 2015; Liu et al., 2004; Easterling et  
288 al., 1997). Although previous studies have indicated that the microclimate (e.g. urban  
289 heat island) has a larger effect on minimum temperatures because of the lower and more  
290 stable boundary layer at night (Zhou and Ren, 2011; Christy et al., 2009), many  
291 investigators argue that variability in  $R_s$  is the primary reason for the daily contrast in  
292 warming rates (Sanchez-Lorenzo and Wild, 2012; Makowski et al., 2009).

### 293 **3.1.2. Spatial patterns in temperature variability**

294 As shown in Fig 4, clear spatial heterogeneity was demonstrated in the warming  
295 rates for  $T_{s-max}$  and  $T_{a-max}$  in China from 1960 to 2003. The trends of  $T_{s-max}$  and  $T_{a-max}$   
296 were statistically higher for the Tibet Plateau, and Northwest and Northeast China (see  
297 Fig S6) compared with the North China Plain and South China. Cooling trends in  $T_{s-max}$   
298 even detected for the Sichuan Basin, the Yangtze River Delta, and the Pearl River Delta.  
299 Lower rates of warming of  $T_{a-max}$  in South China and the North China Plain have also  
300 been previously reported (Liu et al., 2004; Li et al., 2015).

301 The warming rates of  $T_{s-max}$  and  $T_{a-max}$  in South China and the North China Plain  
302 in the warm seasons were considerably lower than those in the cold seasons, which

303 resulted in stronger spatial heterogeneity in the warm seasons (Fig 4b and 4h). The  
304 spatial and seasonal patterns of  $T_{a-max}$  were similar, although they were not as similar as  
305 the patterns of  $T_{s-max}$ . The spatial contrast in the trends between  $T_{s-min}$  and  $T_{a-min}$  was  
306 much less than that between  $T_{s-max}$  and  $T_{a-max}$ , although a strong dependence on latitude  
307 was observed (Fig 4d and 4j). This dependence has been successfully attributed to  
308 amplified dynamics (Wallace et al., 2012; Ding et al., 2014).

309 The correlation between  $T_s$  and  $T_a$  was highly significant. Based on the time series  
310 of the national mean yearly anomalies (see Fig 2 and Fig 3), the correlation coefficient  
311 between  $T_{s-max}$  and  $T_{a-max}$  was 0.877 and between  $T_{s-min}$  and  $T_{a-min}$  was 0.976 on the  
312 annual scale. In the spatial pattern of the trends (Fig 4), the correlation coefficient  
313 between  $T_{s-max}$  and  $T_{a-max}$  was 0.488 and between  $T_{s-min}$  and  $T_{a-min}$  was 0.638 on the  
314 annual scale. All of these correlations between  $T_s$  and  $T_a$  were significant at the 95%  
315 significance level, which indicated a close relation between  $T_s$  and  $T_a$  for both  
316 interannual fluctuations and secular trends.

317 The correlation between  $T_{s-min}$  and  $T_{a-min}$  was significantly higher than that between  
318  $T_{s-max}$  and  $T_{a-max}$ .  $T_{s-min}$  is closely related to the land-atmosphere longwave wave  
319 radiation balance at night, which is closely associated with the atmospheric greenhouse  
320 effect (Dai et al., 1999). During the day,  $T_s$  is directly determined by the land surface

321 energy balance, i.e., the incoming energy (including  $R_s$ ) and atmospheric longwave  
322 radiation (Wang and Dickinson, 2013a), and it is partitioned into latent and sensible  
323 heat fluxes (Zhou and Wang, 2016). Although  $T_a$  is dependent on the land-atmosphere  
324 sensible heat flux, it is also affected by local and/or large-scale circulation. Thus, the  
325 changes in the land surface energy balance caused by  $R_s$  and  $P$  have different levels of  
326 effect on  $T_s$  and  $T_a$  during the day, which most likely caused the lower correlation  
327 between  $T_{s-max}$  and  $T_{a-max}$  than that between  $T_{s-min}$  and  $T_{a-min}$ .

## 328 **3.2. Effect of $R_s$ and $P$ on temperatures**

### 329 **3.2.1 Effect of $R_s$**

330 As shown in Fig S4,  $R_s$  is closely linked with  $T_{s-max}$  and  $T_{a-max}$  but not with  $T_{s-min}$   
331 and  $T_{a-min}$ , and the correlation between  $T_{s-max}$  and  $R_s$  was higher than that between  $T_{a-max}$   
332 and  $R_s$ . For the seasonal scales, the partial correlation between  $T_{s-max} / T_{a-max}$  and  $R_s$  in  
333 the warm seasons was higher than that in the cold seasons, and this correlation was  
334 stronger in South China and the North China Plain. South China has high soil moisture;  
335 therefore, the relationship between the energy used for evapotranspiration and  $R_s$  is  
336 approximately linear (Wang and Dickinson, 2013b; Zhou et al., 2007). However,  
337 northwest China presents dry soil over most of the year; thus the energy used for  
338 evapotranspiration is more dependent on  $P$ . As a result, the energy available for heating

339 the surface and air temperatures is not as closely correlated with  $R_s$ . Therefore, the  
340 correlation coefficients between  $R_s$  and  $T_{s-max}/T_{a-max}$  were higher in South China.

341 To quantify the effect of  $R_s$  on temperature, the sensitivity of the studied  
342 temperatures to changes in  $R_s$  was calculated (Eq. (1)). As shown in Fig S7 shows,  $T_{s-}$   
343  $_{max}$  was the most sensitive to  $R_s$ , followed by  $T_{a-max}$ , and the national means for  $T_{s-max}$   
344 was  $0.092\pm 0.018\text{ }^\circ\text{C (W m}^{-2}\text{)}^{-1}$  (95% confidence level) and  $T_{a-max}$  was  $0.035\pm 0.010\text{ }^\circ\text{C}$   
345  $(\text{W m}^{-2}\text{)}^{-1}$  (95% confidence level).  $T_{s-min}$  and  $T_{a-min}$  were not sensitive to  $R_s$  because  
346 these temperatures are primarily affected by atmospheric longwave radiation night.

347 Based on the above analysis, we calculated the effect of changes in  $R_s$  on the  
348 studied temperatures. From 1960 to 2003, the calculations of the monthly anomalies at  
349 1,977 stations indicated that the national mean rate of decrease of  $R_s$  was  $-1.502\pm 0.42$   
350  $\text{W m}^{-2}\text{ }10\text{yr}^{-1}$  (95% confidence level), and the trend was significant in most regions of  
351 China (see Fig S8). Our rate of decrease was considerably less than the global average  
352 diminishing rate (from approximately  $-2.3$  to  $-5.1\text{ W m}^{-2}\text{ }10\text{yr}^{-1}$ ) between the 1960s  
353 and the 1990s (Gilgen et al., 1998; Liepert, 2002; Stanhill and Cohen, 2001; Ohmura,  
354 2006) and the national mean dimming rate across China (from approximately  $-2.9$  to  
355  $-5.2\text{ W m}^{-2}\text{ }10\text{yr}^{-1}$ ) between the 1960s and the 2000s based on radiation station  
356 observations (Che et al., 2005; Liang and Xia, 2005; Shi et al., 2008; Wang et al., 2015a).

357 As noted in the data section, the sensitivity drift and replacement of instruments  
358 used for the  $R_s$  observations resulted in a significant homogenization of the station  
359 observation records (Wang, 2014; Wang et al., 2015a), which introduced considerable  
360 uncertainty to the trend estimations. Tang et al. (2011) used quality-controlled  
361 observational data from 72 stations and two radiation models based on 479 stations to  
362 determine that the rate in China decreased from approximately  $-2.1$  to  $-2.3 \text{ W m}^{-2}$   
363  $10\text{yr}^{-1}$  during 1961-2000, and they also showed that  $R_s$  values have remained essentially  
364 unchanged since 2000. These findings are generally consistent with our results.

365 Because of the decreasing trend in  $R_s$ , the national mean warming trends of  $T_{s-max}$   
366 and  $T_{a-max}$  decreased by  $0.139 \text{ }^\circ\text{C } 10\text{yr}^{-1}$  and  $0.053 \text{ }^\circ\text{C } 10\text{yr}^{-1}$ , respectively. Spatially,  
367 the decreasing rate of  $R_s$  in South China and the North China Plain was significantly  
368 higher than that in other regions, particularly in the warm seasons (Fig 5b). Therefore,  
369 the cooling effect of decreasing  $R_s$  on  $T_{s-max}$  and  $T_{a-max}$  was more significant in South  
370 China and the China North Plain, and it resulted in significantly lower warming rates  
371 of  $T_{s-max}$  and  $T_{a-max}$  in those regions than in the other regions (see Figs. 4). The spatial  
372 consistency between the decreasing  $R_s$  trend and the slowdown of  $T_{s-max}/T_{a-max}$  warming  
373 implied that variations in  $R_s$  were the primary reason for the spatial heterogeneity of the  
374 warming rate in  $T_{s-max}/T_{a-max}$ .

### 375 3.2.2 Effect of $P$

376 As shown in Fig S5, a significant negative correlation was detected between  $T_{s-max}$   
377 and  $P$ , and the correlation was more significant in the warm seasons than in the cold  
378 seasons.  $P$  negatively correlated with temperature because  $P$  reduces temperatures by  
379 increasing the surface evaporative cooling (Dai et al., 1997; Wang et al., 2006). The  
380 national mean sensitivities of  $T_{s-max}$  and  $T_{a-max}$  to  $P$  were  $-0.321 \pm 0.098$  °C  $10 \text{ mm}^{-1}$  and  
381  $-0.064 \pm 0.054$  °C  $10 \text{ mm}^{-1}$  (95% confidence level), respectively. As shown in Fig S9,  
382 seasonal and spatial changes in the sensitivity of  $T_{s-max}$  and  $T_{a-max}$  to  $P$  were apparent  
383 (Fig S9a–c and Fig S9g–i). The sensitivities of  $T_{s-max}/T_{a-max}$  were significantly higher in  
384 arid regions (dry seasons) than humid regions (rainy seasons) (Wang and Dickinson,  
385 2013b). As expected,  $T_{s-min}$  and  $T_{a-min}$  were both less sensitive to variations in the  $P$ .

386 The trend in  $P$  from 1960 to 2003 over the 1,977 stations showed obvious spatial  
387 heterogeneities. A slight increasing trend in  $P$  was observed in China during this period  
388 at rate of  $0.112 \pm 0.718$  mm  $10\text{yr}^{-1}$  (95% confidence level). An increasing  $P$  trend was  
389 observed in northwestern China and southeastern China, whereas a decreasing trend  
390 was observed in the North China Plain, the Sichuan Basin, and parts of northeastern  
391 China. However, the  $P$  trends were not significant in most regions (see Fig S8).  
392 Variations in  $P$  significantly differed by season (see Fig 6b and Fig 6c). The seasonal

393 and spatial variations in  $P$  are consistent with those of previous studies (Zhai et al.,  
394 2005; Wang et al., 2015b).

395 For  $T_{a-max}$  and  $T_{s-max}$ , the warming trend in the North China Plain, the Sichuan  
396 Basin, and parts of northeastern China was aggravated by the reduction in  $P$ , whereas  
397 the warming trend in northwestern China and in the Mongolian Plateau were slowed by  
398 increases in  $P$  (Fig 6d). For the national average, the effect of increasing  $P$  resulted in  
399 decreases in the warming trends of  $T_{s-max}$  and  $T_{a-max}$  by  $-0.007$  °C  $10yr^{-1}$  and  $-0.002$  °C  
400  $10yr^{-1}$ , respectively. However, the effect of  $P$  on  $T_{s-max}$  was approximately an order of  
401 magnitude less than that of  $R_s$ .

### 402 **3.3. Trends of surface and air temperature after adjusting for the effect of $R_s$ and** 403 **$P$**

404 Based on the above analysis of the effect of  $R_s$  and  $P$  on temperatures, we found  
405 that variations in  $R_s$  and  $P$  had little effect on  $T_{s-min}$  and  $T_{a-min}$ . However,  $R_s$  and  $P$  had  
406 important effect on the trends of  $T_{s-max}$  and  $T_{a-max}$  (see Fig S3), particularly in central  
407 and South China, where  $T$  was more closely related to  $R_s$  (see Fig S4). Therefore, only  
408 the effects of  $R_s$  and  $P$  on  $T_{s-max}$  and  $T_{a-max}$  were analyzed. After adjusting for the effect  
409 of  $R_s$  and  $P$  (Fig 7), the warming rates of  $T_{s-max}$  and  $T_{a-max}$  increased by  $0.146$  °C  $10yr^{-1}$   
410 ( $64.3\%$ ) and  $0.055$  °C  $10yr^{-1}$  ( $33.0\%$ ), respectively. Additionally, the increasing

411 amplitude of warming rates in the warm seasons was significantly higher than that in  
412 the cold seasons, which resulted in a seasonal contrast in warming rates, with  $T_{s-max}$  and  
413  $T_{a-max}$  decreasing by 45.0% and 17.2% respectively (see Table 1).

414 More importantly, after adjusting for the effect of  $R_s$  and  $P$ , the spatial coherence  
415 of the warming rates of  $T_{s-max}$  and  $T_{a-max}$  in South China and the North China Plain  
416 clearly improved (Fig 8). The regional differences among the North China Plain, South  
417 China, and other regions in China significantly decreased because of the increase in  
418 warming rates in South China and the North China Plain. Additionally, the warming  
419 trends of  $T_{s-max}$  and  $T_{a-max}$  became more statistically significant in the North China Plain  
420 and South China (see 10).

421 To clearly illustrate these changes, we selected two regions in China for further  
422 investigation: R1 primarily included the North China Plain and R2 primarily included  
423 the Loess Plateau (see Fig 9a). Although these regions share the same latitudes, the  
424 trend for  $R_s$  were substantially different (see Fig 9b). After adjusting for the effect of  $R_s$   
425 and  $P$ , the annual trends for  $T_{s-max}$  and  $T_{a-max}$  in R1 increased by 0.304 and 0.118 °C  
426  $10yr^{-1}$ , respectively, whereas those in R2 increased by only 0.025 and 0.016 °C  $10yr^{-1}$ ,  
427 respectively. Therefore, following the adjustment, the differences in the warming rates  
428 of  $T_{s-max}$  and  $T_{a-max}$  between R1 and R2 were significantly reduced (see Fig 9d).

429        Following the adjustment in R1, the seasonal and diurnal differences in the  
430 warming rates of  $T_{s-max}$  and  $T_{a-max}$  significantly decreased. The differences in warming  
431 rates between the warm seasons and cold seasons decreased by 68.7% for  $T_{s-max}$  and by  
432 50.8% for  $T_{a-max}$  after the adjustment. Additionally, the differences in the warming rates  
433 between  $T_{s-max}$  and  $T_{s-min}$  decreased by 93.4% and between  $T_{a-max}$  and  $T_{a-min}$  decreased  
434 by 59.6% in R1. In R2, the adjustment did not significantly change the seasonal and  
435 diurnal differences in temperatures. Overall, the trends for R1 and R2 became more  
436 consistent after adjusting for difference in  $R_s$  and  $P$  (see Fig 9d).

#### 437 **4. Conclusions and Discussion**

438        Although a general warming trends has been observed throughout China, the  
439 regional warming trends show significant spatial and temporal heterogeneity. In this  
440 study, we analyzed the spatial and temporal patterns of  $T_s$  and  $T_a$  from 1960 to 2003  
441 and further analyzed and quantified the effects of  $R_s$  and  $P$  on these temperatures. The  
442 primary results of the study are as follows.

443        The national mean warming rates from 1960 to 2003 of  $T_{s-max}$ ,  $T_{s-min}$ ,  $T_{a-max}$ , and  
444  $T_{a-min}$  were  $0.227\pm 0.091$ ,  $0.315\pm 0.058$ ,  $0.167\pm 0.068$ , and  $0.356\pm 0.057$  °C  $10\text{yr}^{-1}$ ,  
445 respectively. The warming rates of  $T_{s-max}$  and  $T_{a-max}$  in South China and the North China  
446 Plain were significantly lower than those in the other regions, and the spatial

447 heterogeneity in the warm seasons was greater than that in the cold seasons.

448 During the study period, the  $R_s$  value decreased by  $-1.502 \pm 0.042 \text{ W m}^{-2} 10\text{yr}^{-1}$   
449 (95% confidence level), and higher diminishing rates were observed in South China  
450 and the North China Plain. Using a partial regression analysis, we found that  $R_s$  was the  
451 primary cause of the spatial patterns in the warming rates of  $T_{s-max}$  and  $T_{a-max}$ .

452 After adjusting for the effect of  $R_s$  and  $P$ , the warming rates of  $T_{s-max}$  and  $T_{a-max}$  in  
453 South China and the North China Plain significantly increased and the regional  
454 differences in warming rates in China clearly decreased (see Fig 8). After the  
455 adjustments, the warming rates of  $T_{s-max}$  and  $T_{a-max}$  in the North China Plain increased  
456 by  $0.304$  and  $0.118 \text{ }^\circ\text{C } 10\text{yr}^{-1}$ , respectively, whereas those on Loess Plateau increased  
457 only by  $0.025$  and  $0.016 \text{ }^\circ\text{C } 10\text{yr}^{-1}$ , respectively. Therefore, the differences in warming  
458 rates of  $T_{s-max}$  and  $T_{a-max}$  between the North China Plain and the Loess Plateau were  
459 almost eliminated (see Fig 9d).

460 After adjusting for the effect of  $R_s$  and  $P$ , the warming trend of  $T_{s-max}$  increased by  
461  $0.146 \text{ }^\circ\text{C } 10\text{yr}^{-1}$  and that of  $T_{a-max}$  increased by  $0.055 \text{ }^\circ\text{C } 10\text{yr}^{-1}$ . In addition, the trends  
462 of  $T_{s-max}$  and  $T_{a-max}$  became  $0.373 \pm 0.068$  and  $0.222 \pm 0.062 \text{ }^\circ\text{C } 10\text{yr}^{-1}$  respectively.  
463 Reduction in  $R_s$  resulted in decreases in the warming rates of  $T_{s-max}$  and  $T_{a-max}$  by  
464  $0.139 \text{ }^\circ\text{C } 10\text{yr}^{-1}$  and  $0.053 \text{ }^\circ\text{C } 10\text{yr}^{-1}$ , respectively, which accounted for 95.0% and 95.8%

465 of the total effect of  $R_s$  and  $P$ , respectively. For the seasonal contrast, the warming rates  
466 of  $T_{s-max}$  and  $T_{a-max}$  decreased by 45.0% and 17.2%, respectively. For the daily contrast,  
467 the warming rates of  $T_s$  and  $T_a$  decreased by 33.0% and 29.1%, respectively.

468 In addition to  $R_s$  and  $P$ , temperature warming rates may be affected by many other  
469 factors, such as land cover and land use changes; however those factors have not been  
470 discussed in this study because of lack of data (Liu et al., 2005; Zhang et al., 2016).  
471 After adjusting for the effect of changes in  $R_s$  and  $P$  changes, the spatial differences in  
472 the warming trends clearly decreased; however, certain regional differences remained.  
473 The warming rate of  $T_{s-max}$  in the Sichuan Basin remained significantly lower than that  
474 in other regions after adjusting for these effects. Additionally, the differences in the  
475 warming rates of  $T_{s-min}$  and  $T_{a-min}$  between the northern and southern areas were not  
476 explained by the effects of  $R_s$  and  $P$ ; further study is required.

477 **Acknowledgements** The National Natural Science Foundation of China (41525018  
478 and 91337111) and the National Basic Research Program of China funded this study.  
479 The land surface temperatures and sunshine duration datasets that include data from  
480 approximately 2,400 meteorological stations in China from 1960 to 2003, are obtained  
481 from the China Meteorological Administration (CMA, <http://data.cma.gov.cn/data>).

482 **References**

- 483 Ait-Mesbah, S., Dufresne, J. L., Cheruy, F., and Hourdin, F.: The role of thermal inertia in the  
484 representation of mean and diurnal range of surface temperature in semiarid and arid  
485 regions, *Geophys Res Lett*, 42, 7572-7580, 10.1002/2015gl065553, 2015.
- 486 Bounoua, L., Collatz, G. J., Sellers, P. J., Randall, D. A., Dazlich, D. A., Los, S. O., Berry, J.  
487 A., Fung, I., Tucker, C. J., Field, C. B., and Jensen, T. G.: Interactions between vegetation  
488 and climate: Radiative and physiological effects of doubled atmospheric CO<sub>2</sub>, *J Climate*,  
489 12, 309-324, 10.1175/1520-0442(1999)012<0309:ibvacr>2.0.co;2, 1999.
- 490 Boyles, R. P., and Raman, S.: Analysis of climate trends in North Carolina (1949-1998),  
491 *Environ Int*, 29, 263-275, 10.1016/s0160-4120(02)00185-x, 2003.
- 492 Campbell, G. G., and VonderHaar, T. H.: Comparison of surface temperature minimum and  
493 maximum and satellite measured cloudiness and radiation budget, *J Geophys Res-Atmos*,  
494 102, 16639-16645, 10.1029/96jd02718, 1997.
- 495 Cao, L., Zhu, Y., Tang, G., Yuan, F., and Yan, Z.: Climatic warming in China according to a  
496 homogenized data set from 2419 stations, *Int J Climatol*, 36, 4384-4392, 10.1002/joc.4639,  
497 2016.
- 498 Che, H. Z., Shi, G. Y., Zhang, X. Y., Arimoto, R., Zhao, J. Q., Xu, L., Wang, B., and Chen, Z.  
499 H.: Analysis of 40 years of solar radiation data from China, 1961-2000, *Geophys Res Lett*,  
500 32, 10.1029/2004gl022322, 2005.
- 501 Chen, H. S., Ma, H. D., Li, X., and Sun, S. L.: Solar influences on spatial patterns of Eurasian  
502 winter temperature and atmospheric general circulation anomalies, *J Geophys Res-Atmos*,  
503 120, 8642-8657, 10.1002/2015jd023415, 2015.
- 504 Cheng, Z., Wang, S., Fu, X., Watson, J. G., Jiang, J., Fu, Q., Chen, C., Xu, B., Yu, J., Chow, J.  
505 C., and Hao, J.: Impact of biomass burning on haze pollution in the Yangtze River delta,  
506 China: a case study in summer 2011, *Atmos. Chem. Phys.*, 14, 4573-4585, 10.5194/acp-  
507 14-4573-2014, 2014.
- 508 Christy, J. R., Norris, W. B., and McNider, R. T.: Surface Temperature Variations in East Africa  
509 and Possible Causes, *J Climate*, 22, 3342-3356, 10.1175/2008jcli2726.1, 2009.

- 510 Dai, A., DelGenio, A. D., and Fung, I. Y.: Clouds, precipitation and temperature range, *Nature*,  
511 386, 665-666, 10.1038/386665b0, 1997.
- 512 Dai, A., Trenberth, K. E., and Karl, T. R.: Effects of clouds, soil moisture, precipitation, and  
513 water vapor on diurnal temperature range, *J Climate*, 12, 2451-2473, 10.1175/1520-  
514 0442(1999)012<2451:eocsmp>2.0.co;2, 1999.
- 515 Ding, Q., Wallace, J. M., Battisti, D. S., Steig, E. J., Gallant, A. J. E., Kim, H.-J., and Geng, L.:  
516 Tropical forcing of the recent rapid Arctic warming in northeastern Canada and Greenland,  
517 *Nature*, 509, 209+, 10.1038/nature13260, 2014.
- 518 Duan, A., and Xiao, Z.: Does the climate warming hiatus exist over the Tibetan Plateau?, *Sci.*  
519 *Rep*, 5, 10.1038/srep13711, 2015.
- 520 Easterling, D. R., Horton, B., Jones, P. D., Peterson, T. C., Karl, T. R., Parker, D. E., Salinger,  
521 M. J., Razuvayev, V., Plummer, N., Jamason, P., and Folland, C. K.: Maximum and  
522 minimum temperature trends for the globe, *Science*, 277, 364-367,  
523 10.1126/science.277.5324.364, 1997.
- 524 Falge, E., Reth, S., Bruggemann, N., Butterbach-Bahl, K., Goldberg, V., Oltchev, A., Schaaf,  
525 S., Spindler, G., Stiller, B., Queck, R., Kostner, B., and Bernhofer, C.: Comparison of  
526 surface energy exchange models with eddy flux data in forest and grassland ecosystems  
527 of Germany, *Ecol Model*, 188, 174-216, 10.1016/j.ecolmodel.2005.01.057, 2005.
- 528 Gettelman, A., and Fu, Q.: Observed and simulated upper-tropospheric water vapor feedback,  
529 *J Climate*, 21, 3282-3289, 10.1175/2007jcli2142.1, 2008.
- 530 Gilgen, H., Wild, M., and Ohmura, A.: Means and trends of shortwave irradiance at the surface  
531 estimated from global energy balance archive data, *J Climate*, 11, 2042-2061,  
532 10.1175/1520-0442-11.8.2042, 1998.
- 533 Hartmann, D. L., Ramanathan, V., Berroir, A., and Hunt, G. E.: Earth radiation budget data and  
534 climate research, *Rev Geophys*, 24, 439-468, 10.1029/RG024i002p00439, 1986.
- 535 Hartmann, D. L., Tank, A. M. G. K., and Rusticucci, M.: *Observation: Atmosphere and surface*,  
536 IPCC, 1533 pp, 10.1017/CBO09781107415324, 2013.
- 537 Hegerl, G. C., and Zwiers, F. W.: *Climate change 2007: Understanding and attributing climate*  
538 *change*, Cambridge University Press, 1007 pp., 2007.

- 539 Hingray, B., Mezghani, A., and Buishand, T. A.: Development of probability distributions for  
540 regional climate change from uncertain global mean warming and an uncertain scaling  
541 relationship, *Hydrol Earth Syst Sc*, 11, 1097-1114, 2007.
- 542 Huang, J., Guan, X., and Ji, F.: Enhanced cold-season warming in semi-arid regions, *Atmos.*  
543 *Chem. Phys.*, 12, 5391-5398, 10.5194/acp-12-5391-2012, 2012.
- 544 Jones, P. D., and Moberg, A.: Hemispheric and large-scale surface air temperature variations:  
545 An extensive revision and an update to 2001, *J Climate*, 16, 206-223, 10.1175/1520-  
546 0442(2003)016<0206:halssa>2.0.co;2, 2003.
- 547 Kalnay, E., and Cai, M.: Impact of urbanization and land-use change on climate, *Nature*, 423,  
548 528-531, 10.1038/nature01675, 2003.
- 549 Karl, T. R., Kukla, G., Razuvayev, V. N., Changery, M. J., Quayle, R. G., Heim, R. R., Easterling,  
550 D. R., and Fu, C. B.: Global warming - evidence for asymmetric diurnal temperature-  
551 change, *Geophys Res Lett*, 18, 2253-2256, 10.1029/91gl02900, 1991.
- 552 Karoly, D. J., and Stott, P. A.: Anthropogenic warming of central England temperature, *Atmos.*  
553 *Sci. Lett.*, 7, 81-85, 10.1002/asl.136, 2006.
- 554 Kukla, G., and Karl, T. R.: Nighttime warming and the greenhouse-effect, *Environ Sci Technol*,  
555 27, 1468-1474, 10.1021/es00045a001, 1993.
- 556 Lauritsen, R. G., and Rogers, J. C.: US Diurnal Temperature Range Variability and Regional  
557 Causal Mechanisms, 1901-2002, *J Climate*, 25, 7216-7231, 10.1175/jcli-d-11-00429.1,  
558 2012.
- 559 Li, B. F., Chen, Y. N., and Shi, X.: Why does the temperature rise faster in the arid region of  
560 northwest China?, *J Geophys Res-Atmos*, 117, 10.1029/2012jd017953, 2012.
- 561 Li, Q. X., Yang, S., Xu, W. H., Wang, X. L. L., Jones, P., Parker, D., Zhou, L. M., Feng, Y., and  
562 Gao, Y.: China experiencing the recent warming hiatus, *Geophys Res Lett*, 42, 889-898,  
563 10.1002/2014gl062773, 2015.
- 564 Liang, F., and Xia, X. A.: Long-term trends in solar radiation and the associated climatic factors  
565 over China for 1961-2000, *Ann Geophys*, 23, 2425-2432, 2005.
- 566 Liepert, B. G.: Observed reductions of surface solar radiation at sites in the United States and

- 567 worldwide from 1961 to 1990, *Geophys Res Lett*, 29, 10.1029/2002gl014910, 2002.
- 568 Lim, Y. K., Cai, M., Kalnay, E., and Zhou, L. M.: Observational evidence of sensitivity of  
569 surface climate changes to land types and urbanization, *Geophys Res Lett*, 32, 4,  
570 10.1029/2005gl024267, 2005.
- 571 Liu, B. H., Xu, M., Henderson, M., Qi, Y., and Li, Y. Q.: Taking China's temperature: Daily  
572 range, warming trends, and regional variations, 1955-2000, *J Climate*, 17, 4453-4462,  
573 10.1175/3230.1, 2004.
- 574 Liu, J. Y., Liu, M. L., Tian, H. Q., Zhuang, D. F., Zhang, Z. X., Zhang, W., Tang, X. M., and  
575 Deng, X. Z.: Spatial and temporal patterns of China's cropland during 1990-2000: An  
576 analysis based on Landsat TM data, *Remote Sens Environ*, 98, 442-456,  
577 10.1016/j.rse.2005.08.012, 2005.
- 578 Mahlstein, I., and Knutti, R.: Regional climate change patterns identified by cluster analysis,  
579 *Clim Dynam*, 35, 587-600, 10.1007/s00382-009-0654-0, 2010.
- 580 Makowski, K., Jaeger, E. B., Chiacchio, M., Wild, M., Ewen, T., and Ohmura, A.: On the  
581 relationship between diurnal temperature range and surface solar radiation in Europe, *J*  
582 *Geophys Res-Atmos*, 114, 16, 10.1029/2008jd011104, 2009.
- 583 Manara, V., Beltrano, M. C., Brunetti, M., Maugeri, M., Sanchez-Lorenzo, A., Simolo, C., and  
584 Sorrenti, S.: Sunshine duration variability and trends in Italy from homogenized  
585 instrumental time series (1936-2013), *J Geophys Res-Atmos*, 120, 3622-3641,  
586 10.1002/2014jd022560, 2015.
- 587 Mariotti, L., Coppola, E., Sylla, M. B., Giorgi, F., and Piani, C.: Regional climate model  
588 simulation of projected 21st century climate change over an all-Africa domain:  
589 Comparison analysis of nested and driving model results, *J Geophys Res-Atmos*, 116,  
590 10.1029/2010jd015068, 2011.
- 591 Menon, S., Hansen, J., Nazarenko, L., and Luo, Y. F.: Climate effects of black carbon aerosols  
592 in China and India, *Science*, 297, 2250-2253, 10.1126/science.1075159, 2002.
- 593 Ohmura, A.: Observed long-term variations of solar irradiance at the earth's surface, *Space Sci*  
594 *Rev*, 125, 111-128, 10.1007/s11214-006-9050-9, 2006.
- 595 Peng, S. S., Piao, S. L., Zeng, Z. Z., Ciais, P., Zhou, L. M., Li, L. Z. X., Myneni, R. B., Yin, Y.,

- 596 and Zeng, H.: Afforestation in China cools local land surface temperature, P Natl Acad Sci  
597 USA, 111, 2915-2919, 10.1073/pnas.1315126111, 2014.
- 598 Ren, G., Xu, M., Chu, Z., Guo, J., Li, Q., Liu, X., and Wang, Y.: Changes of Surface Air  
599 Temperature in China During 1951-2004, Climatic and environmental research, 10, 717-  
600 727, 2005.
- 601 Roy, I., and Haigh, J. D.: The influence of solar variability and the quasi-biennial oscillation on  
602 lower atmospheric temperatures and sea level pressure, Atmos. Chem. Phys., 11, 11679-  
603 11687, 10.5194/acp-11-11679-2011, 2011.
- 604 Sanchez-Lorenzo, A., and Wild, M.: Decadal variations in estimated surface solar radiation over  
605 Switzerland since the late 19th century, Atmos. Chem. Phys., 12, 8635-8644, 10.5194/acp-  
606 12-8635-2012, 2012.
- 607 Seneviratne, S. I., Corti, T., Davin, E. L., Hirschi, M., Jaeger, E. B., Lehner, I., Orlowsky, B.,  
608 and Teuling, A. J.: Investigating soil moisture-climate interactions in a changing climate:  
609 A review, Earth-sci Rev, 99, 125-161, 10.1016/j.earscirev.2010.02.004, 2010.
- 610 Shen, D. J., and Varis, O.: Climate change in China, Ambio, 30, 381-383, 10.1639/0044-  
611 7447(2001)030[0381:ccic]2.0.co;2, 2001.
- 612 Shen, M. G., Piao, S. L., Jeong, S. J., Zhou, L. M., Zeng, Z. Z., Ciais, P., Chen, D. L., Huang,  
613 M. T., Jin, C. S., Li, L. Z. X., Li, Y., Myneni, R. B., Yang, K., Zhang, G. X., Zhang, Y. J.,  
614 and Yao, T. D.: Evaporative cooling over the Tibetan Plateau induced by vegetation growth,  
615 P Natl Acad Sci USA, 112, 9299-9304, 10.1073/pnas.1504418112, 2015.
- 616 Shen, X. J., Liu, B. H., Li, G. D., Wu, Z. F., Jin, Y. H., Yu, P. J., and Zhou, D. W.: Spatiotemporal  
617 change of diurnal temperature range and its relationship with sunshine duration and  
618 precipitation in China, J Geophys Res-Atmos, 119, 13163-13179, 10.1002/2014jd022326,  
619 2014.
- 620 Shi, G. Y., Hayasaka, T., Ohmura, A., Chen, Z. H., Wang, B., Zhao, J. Q., Che, H. Z., and Xu,  
621 L.: Data quality assessment and the long-term trend of ground solar radiation in China, J.  
622 Appl. Meteorol. Clim., 47, 1006-1016, 10.1175/2007jamc1493.1, 2008.
- 623 Stanhill, G., and Cohen, S.: Global dimming: a review of the evidence for a widespread and  
624 significant reduction in global radiation with discussion of its probable causes and possible  
625 agricultural consequences, Agr Forest Meteorol, 107, 255-278, 10.1016/s0168-

- 626 1923(00)00241-0, 2001.
- 627 Sun, Y., Zhang, X. B., Ren, G. Y., Zwiers, F. W., and Hu, T.: Contribution of urbanization to  
628 warming in China, *Nature Climate Change*, 6, 706-+, 10.1038/nclimate2956, 2016.
- 629 Tang, W. J., Yang, K., Qin, J., Cheng, C. C. K., and He, J.: Solar radiation trend across China  
630 in recent decades: a revisit with quality-controlled data, *Atmos. Chem. Phys.*, 11, 393-406,  
631 10.5194/acp-11-393-2011, 2011.
- 632 Taylor, J. R., Randel, W. J., and Jensen, E. J.: Cirrus cloud-temperature interactions in the  
633 tropical tropopause layer: a case study, *Atmos. Chem. Phys.*, 11, 10085-10095,  
634 10.5194/acp-11-10085-2011, 2011.
- 635 Tebaldi, C., Smith, R. L., Nychka, D., and Mearns, L. O.: Quantifying uncertainty in projections  
636 of regional climate change: A Bayesian approach (vol 18, pg 1524, 2005), *J Climate*, 18,  
637 3405-3405, 10.1175/JCLI9001.1a, 2005.
- 638 Vautard, R., Yiou, P., and van Oldenborgh, G. J.: Decline of fog, mist and haze in Europe over  
639 the past 30 years, *Nat Geosci*, 2, 115-119, 10.1038/ngeo414, 2009.
- 640 Vose, R. S., Easterling, D. R., and Gleason, B.: Maximum and minimum temperature trends for  
641 the globe: An update through 2004, *Geophys Res Lett*, 32, 10.1029/2005gl024379, 2005.
- 642 Wallace, J. M., Fu, Q., Smoliak, B. V., Lin, P., and Johanson, C. M.: Simulated versus observed  
643 patterns of warming over the extratropical Northern Hemisphere continents during the  
644 cold season, *P Natl Acad Sci USA*, 109, 14337-14342, 10.1073/pnas.1204875109, 2012.
- 645 Wang, K., and Dickinson, R. E.: Global atmospheric downward longwave radiation at the  
646 surface from ground-based observations, satellite retrievals, and reanalyses, *Rev Geophys*,  
647 51, 150-185, 10.1002/rog.20009, 2013a.
- 648 Wang, K., and Dickinson, R. E.: Contribution of solar radiation to decadal temperature  
649 variability over land, *P Natl Acad Sci USA*, 110, 14877-14882, 10.1073/pnas.1311433110,  
650 2013b.
- 651 Wang, K. C., Li, Z. Q., and Cribb, M.: Estimation of evaporative fraction from a combination  
652 of day and night land surface temperatures and NDVI: A new method to determine the  
653 Priestley-Taylor parameter, *Remote Sens Environ*, 102, 293-305,  
654 10.1016/j.rse.2006.02.007, 2006.

- 655 Wang, K. C., and Dickinson, R. E.: A review of global terrestrial evapotranspiration:  
656 Observation, modeling, climatology, and climatic variability, *Rev Geophys*, 50,  
657 10.1029/2011rg000373, 2012.
- 658 Wang, K. C., Dickinson, R. E., Wild, M., and Liang, S.: Atmospheric impacts on climatic  
659 variability of surface incident solar radiation, *Atmos. Chem. Phys.*, 12, 9581-9592,  
660 10.5194/acp-12-9581-2012, 2012.
- 661 Wang, K. C.: Measurement Biases Explain Discrepancies between the Observed and Simulated  
662 Decadal Variability of Surface Incident Solar Radiation, *Sci. Rep*, 4, 10.1038/srep06144,  
663 2014.
- 664 Wang, K. C., Ma, Q., Li, Z. J., and Wang, J. K.: Decadal variability of surface incident solar  
665 radiation over China: Observations, satellite retrievals, and reanalyses, *J Geophys Res-*  
666 *Atmos*, 120, 6500-6514, 10.1002/2015jd023420, 2015a.
- 667 Wang, K. C., and Zhou, C. L. E.: Regional Contrasts of the Warming Rate over Land  
668 Significantly Depend on the Calculation Methods of Mean Air Temperature, *Sci. Rep*, 5,  
669 10.1038/srep12324, 2015.
- 670 Wang, X., Wang, K., and Su, L.: Contribution of Atmospheric Diffusion Conditions to the  
671 Recent Improvement in Air Quality in China, *Sci. Rep*, 6, 36404, 10.1038/srep36404, 2016.
- 672 Wang, Y. J., Chen, X. Y., and Yan, F.: Spatial and temporal variations of annual precipitation  
673 during 1960-2010 in China, *Quatern Int*, 380, 5-13, 10.1016/j.quaint.2014.12.047, 2015b.
- 674 Weng, Q. H., Lu, D. S., and Schubring, J.: Estimation of land surface temperature-vegetation  
675 abundance relationship for urban heat island studies, *Remote Sens Environ*, 89, 467-483,  
676 10.1016/j.rse.2003.11.005, 2004.
- 677 Wild, M., Ohmura, A., and Makowski, K.: Impact of global dimming and brightening on global  
678 warming, *Geophys Res Lett*, 34, 10.1029/2006gl028031, 2007.
- 679 Wild, M.: Enlightening global dimming and brightening, *B Am Meteorol Soc*, 93, 27-37,  
680 10.1175/bams-d-11-00074.1, 2012.
- 681 Xia, X.: A closer looking at dimming and brightening in China during 1961-2005, *Ann Geophys*,  
682 28, 1121-1132, 10.5194/angeo-28-1121-2010, 2010.

- 683 Yang, K., Koike, T., and Ye, B. S.: Improving estimation of hourly, daily, and monthly solar  
684 radiation by importing global data sets, *Agr Forest Meteorol*, 137, 43-55,  
685 10.1016/j.agrformet.2006.02.001, 2006.
- 686 Yin, Z., Wang, H., and Chen, H.: Understanding Severe Winter Haze Pollution in the North-  
687 Central North China Plain in 2014, *Atmos. Chem. Phys.*, 2016, 1-27, 10.5194/acp-2016-  
688 641, 2016.
- 689 You, Q. L., Min, J. Z., Jiao, Y., Sillanpaa, M., and Kang, S. C.: Observed trend of diurnal  
690 temperature range in the Tibetan Plateau in recent decades, *Int J Climatol*, 36, 2633-2643,  
691 10.1002/joc.4517, 2016.
- 692 Zhai, P. M., Zhang, X. B., Wan, H., and Pan, X. H.: Trends in total precipitation and frequency  
693 of daily precipitation extremes over China, *J Climate*, 18, 1096-1108, 10.1175/jcli-3318.1,  
694 2005.
- 695 Zhang, X., Sun, Y., Mao, W., Liu, Y., and Ren, Y.: Regional Response of Temperature Change  
696 in the Arid Regions of China to Global Warming, *Arid Zone Research*, 27, 592-599, 2010.
- 697 Zhang, Z. X., Li, N., Wang, X., Liu, F., and Yang, L. P.: A Comparative Study of Urban  
698 Expansion in Beijing, Tianjin and Tangshan from the 1970s to 2013, *Remote. Sen.*, 8, 22,  
699 10.3390/rs8060496, 2016.
- 700 Zhou, C. L., and Wang, K. C.: Coldest Temperature Extreme Monotonically Increased and  
701 Hottest Extreme Oscillated over Northern Hemisphere Land during Last 114 Years, *Sci.*  
702 *Rep*, 6, 10.1038/srep25721, 2016.
- 703 Zhou, L. M., Dickinson, R. E., Tian, Y. H., Fang, J. Y., Li, Q. X., Kaufmann, R. K., Tucker, C.  
704 J., and Myneni, R. B.: Evidence for a significant urbanization effect on climate in China,  
705 *P Natl Acad Sci USA*, 101, 9540-9544, 10.1073/pnas.0400357101, 2004.
- 706 Zhou, L. M., Dickinson, R. E., Tian, Y. H., Vose, R. S., and Dai, Y. J.: Impact of vegetation  
707 removal and soil aridation on diurnal temperature range in a semiarid region: Application  
708 to the Sahel, *P Natl Acad Sci USA*, 104, 17937-17942, 10.1073/pnas.0700290104, 2007.
- 709 Zhou, L. M., Dai, A., Dai, Y. J., Vose, R., Zou, C. Z., Tian, Y. H., and Chen, H. S.: Spatial  
710 dependence of diurnal temperature range trends on precipitation from 1950 to 2004, *Clim*  
711 *Dynam*, 32, 429-440, 10.1007/s00382-008-0387-5, 2009.

712 Zhou, L. M., Dickinson, R. E., Dai, A. G., and Dirmeyer, P.: Detection and attribution of  
713 anthropogenic forcing to diurnal temperature range changes from 1950 to 1999:  
714 comparing multi-model simulations with observations, *Clim Dynam*, 35, 1289-1307,  
715 10.1007/s00382-009-0644-2, 2010.

716 Zhou, Y. Q., and Ren, G. Y.: Change in extreme temperature event frequency over mainland  
717 China, 1961-2008, *Climate Res*, 50, 125-139, 10.3354/cr01053, 2011.

718

719

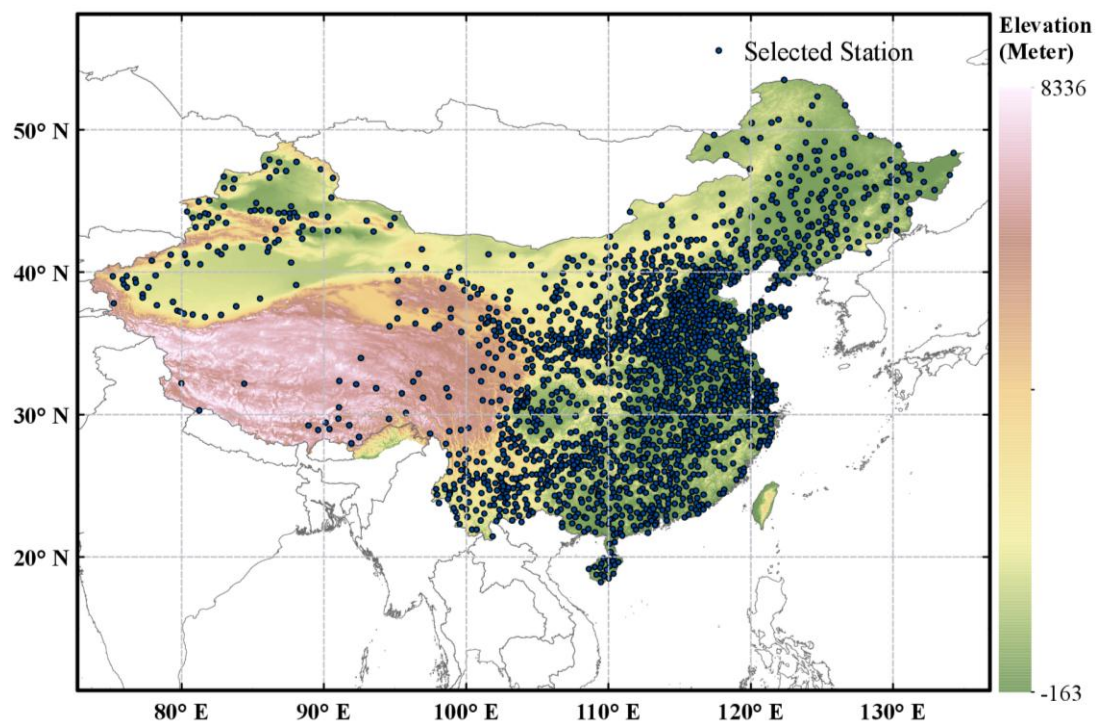
720

721

722

723

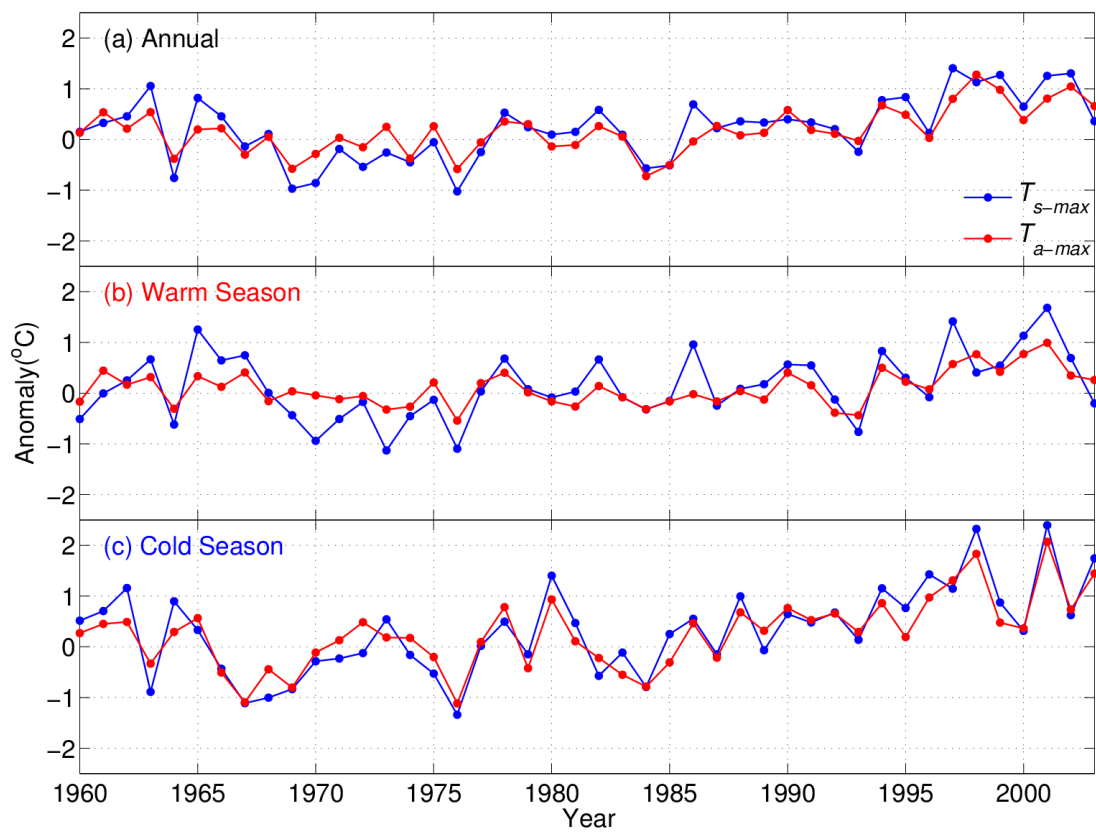
724



725

726 Figure 1. Elevation maps of mainland China and spatial distribution of the 1977  
 727 meteorological stations used in this study. The datasets were provided by China's  
 728 National Meteorological Information Centre (You et al., 2016)  
 729 (<http://data.cma.gov.cn/data>).

730

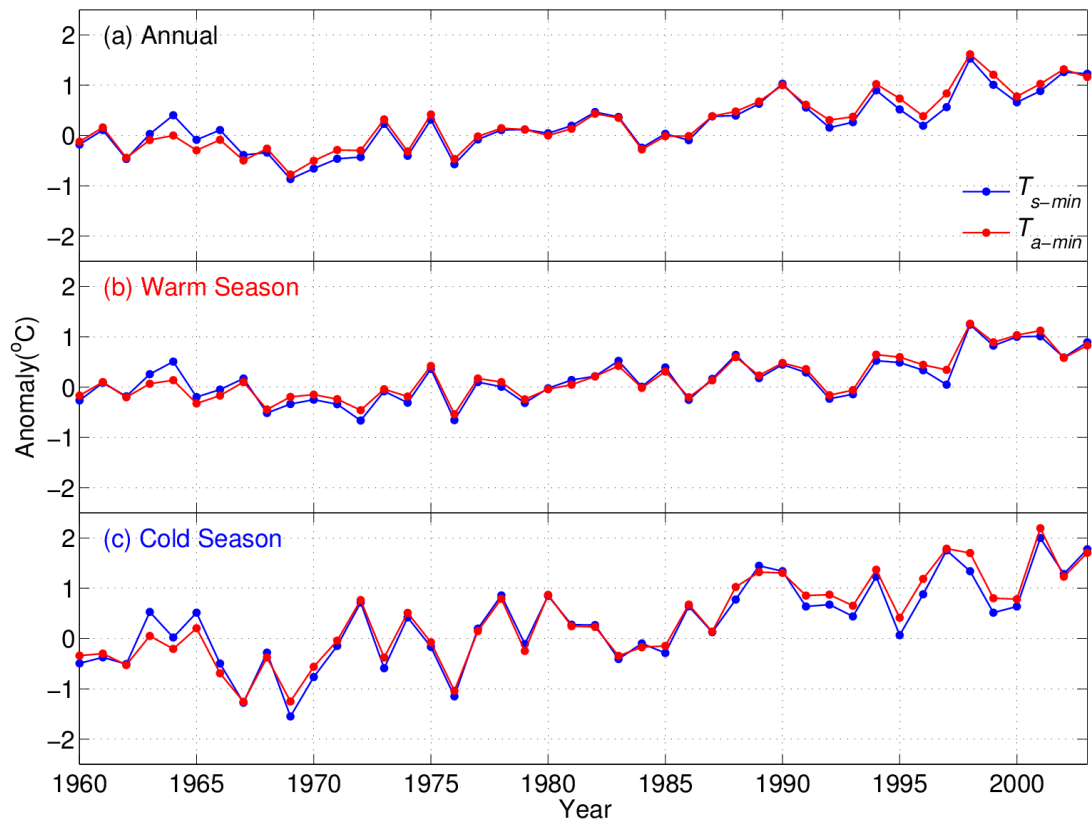


731

732 Figure 2. National mean yearly anomalies of daily maximum land surface temperature

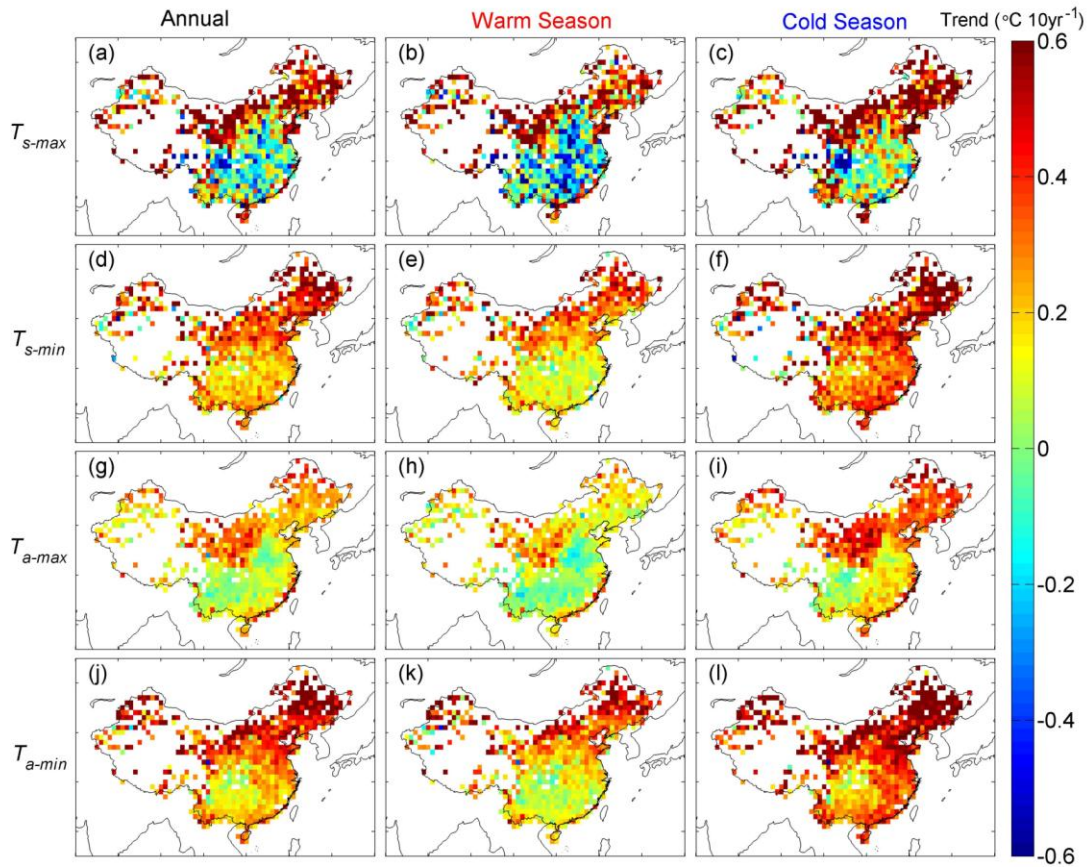
733 ( $T_{s-max}$ , blue line) and daily maximum air temperature ( $T_{a-max}$ , red line) for the annual

734 (a), warm (b), and cold (c) seasonal scales for the reference period from 1961 to 1990.



735

736 Figure 3. National mean yearly anomalies of daily minimum land surface temperature  
 737 ( $T_{s-min}$ , blue line) and daily minimum air temperature ( $T_{a-min}$ , red line) for the annual (a),  
 738 warm (b), and cold (c) seasonal scales for the reference period 1961-1990.

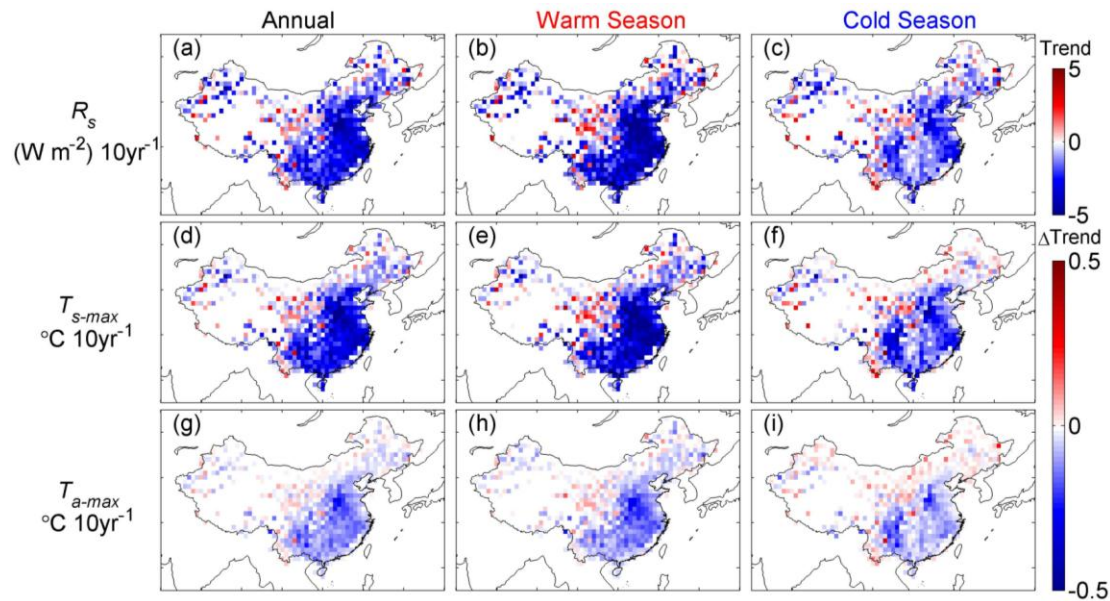


739

740 Figure 4. Maps of the trends of the monthly anomalies for daily maximum land surface  
 741 temperature ( $T_{s-max}$ , a–c), daily minimum land surface temperature ( $T_{s-min}$ , d–f), daily  
 742 maximum air temperature ( $T_{a-max}$ , g–i), and daily minimum air temperature ( $T_{a-min}$ , j–l)  
 743 for the annual, warm (May–October), and cold (November–next April) seasonal scales.

744 All trends reported in these figures were calculated using a linear regression based on  
 745 the least square method.

746

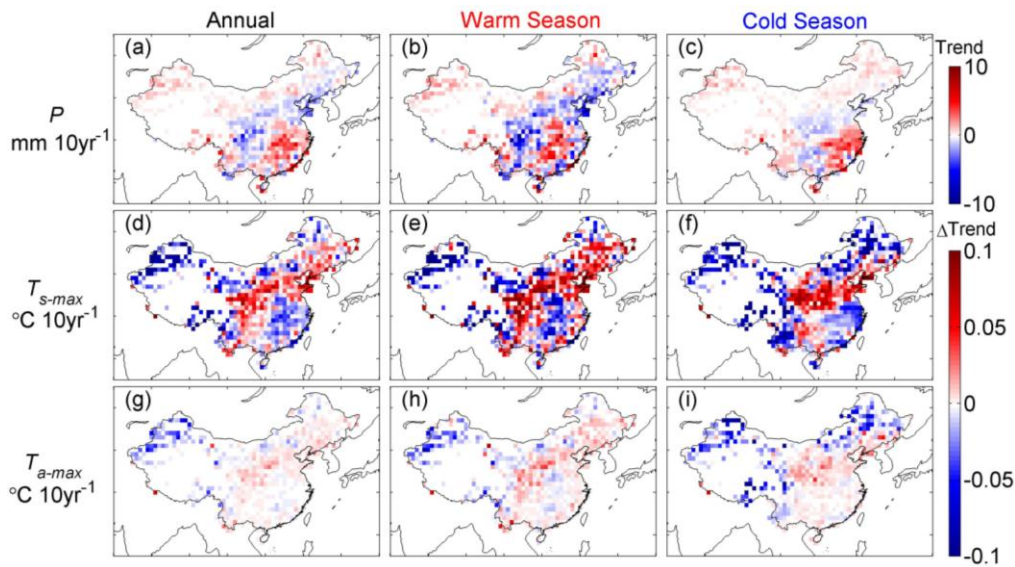


747

748 Figure 5. Maps of the trends in surface solar radiation ( $R_s$ , a–c) and its effect on the  
 749 warming rates of daily maximum land surface temperature ( $T_{s-max}$ , d–f) and daily  
 750 maximum air temperature ( $T_{a-max}$ , g–i). The first line (a–c) is the trend of  $R_s$  from 1960–  
 751 2003; the second line (d–f) and the third line (g–i) are the trend changes caused by  
 752 secular variations of  $R_s$  on  $T_{s-max}$  and  $T_{a-max}$ . Eq (1) was used to strip away the effect of  
 753  $R_s$  on temperatures, and we calculated the trend difference ( $\Delta$ Trend, d–i) between the  
 754 time series of temperatures before and after adjusting for the effect of  $R_s$ . Finally, the  
 755 effect of  $R_s$  on the trends of  $T_{s-max}/T_{a-max}$  was quantified and analyzed (section 3.2.1).

756

757

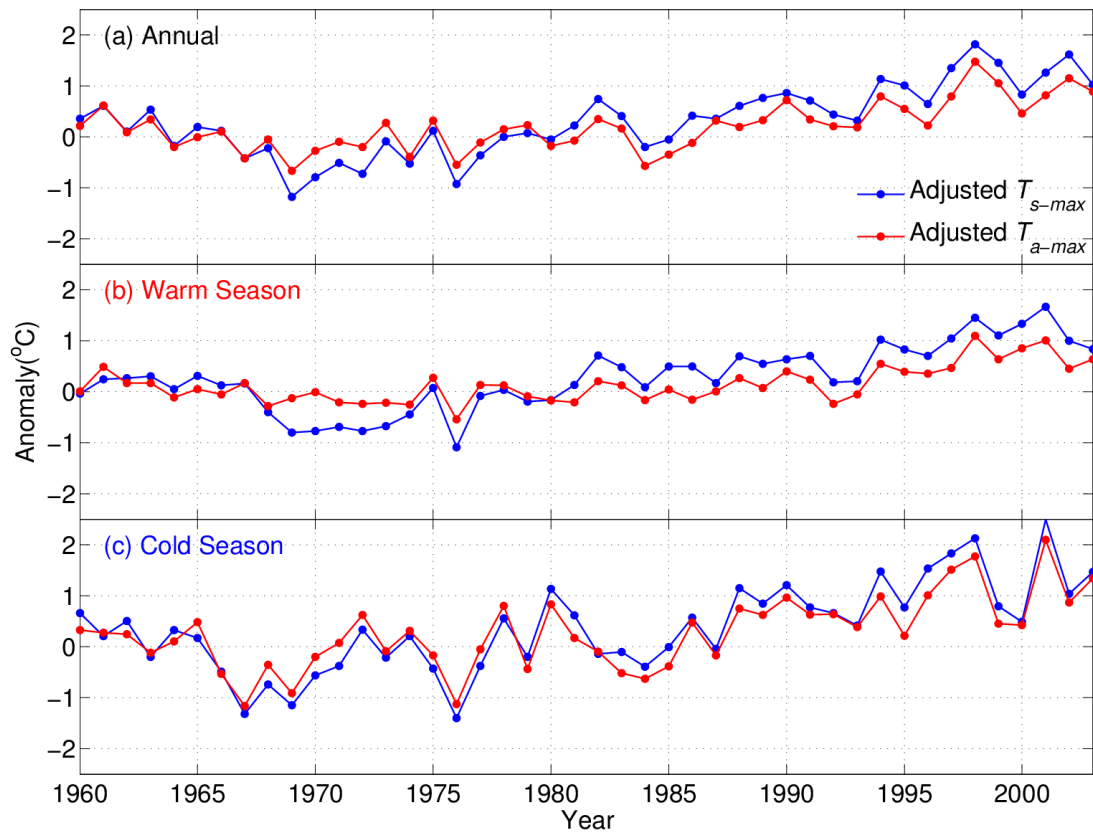


758

759 Figure 6. Maps of the trends in precipitation ( $P$ ) (a–c) and their effect on the warming  
 760 rates for daily maximum land surface temperature ( $T_{s-max}$ , d–f) and daily maximum air  
 761 temperature ( $T_{a-max}$ , g–i). The first line (a–c) is the trend of  $P$  during 1960–2003; the  
 762 second line (d–f) and the third line (g–i) are the trend changes caused by secular  
 763 variations of  $P$  on  $T_{s-max}$  and  $T_{a-max}$ . We used Eq (1) to remove the effects of  $P$  on the  
 764 temperatures, then calculated the trend difference ( $\Delta$ Trend, d–i) between the time series  
 765 of temperatures before and after adjusting for the effect of  $P$ . Finally, the effect of  $P$  on  
 766 the trends of  $T_{s-max}/T_{a-max}$  was quantified and analyzed (section 3.2.2).

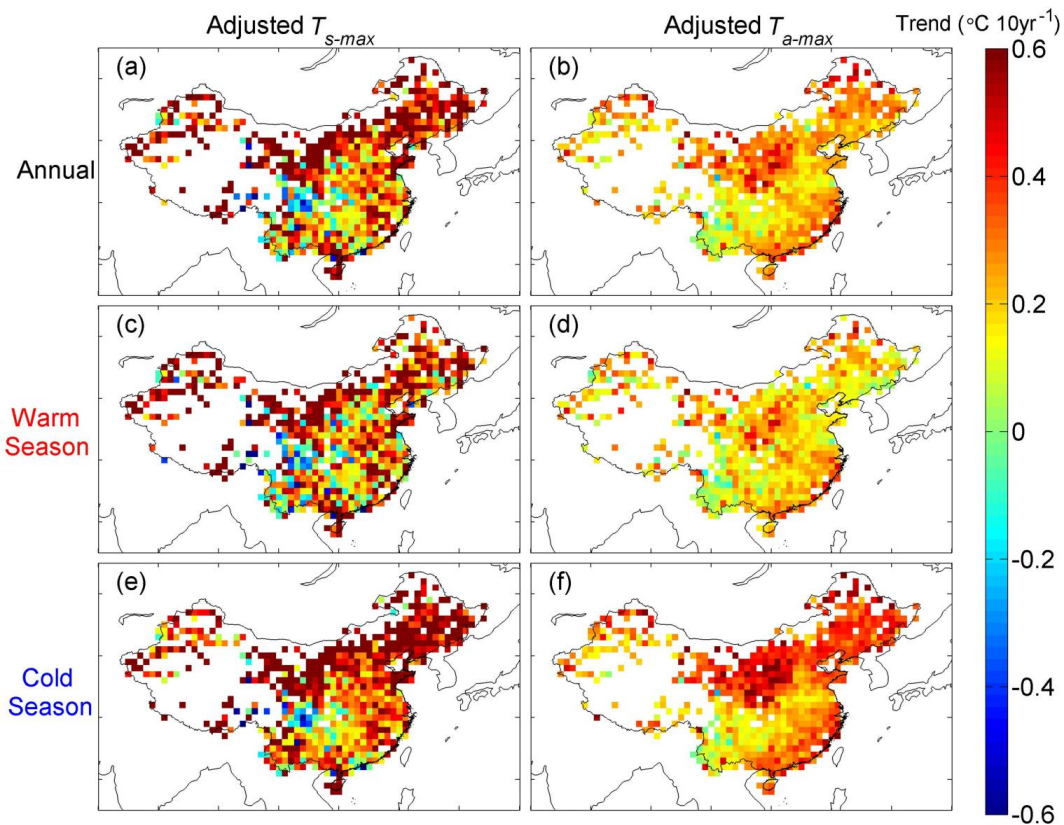
767

768



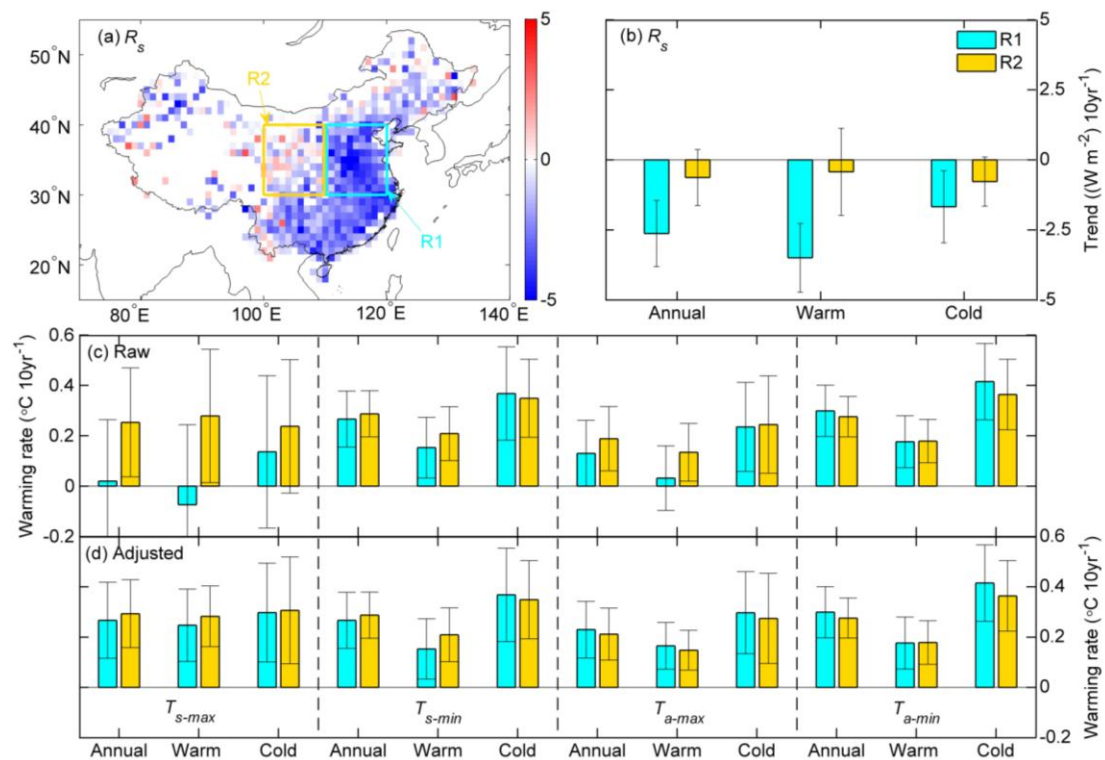
769

770 Figure 7. Regional average anomalies of daily maximum land surface temperature ( $T_{s-max}$ , blue line) and daily maximum air temperature ( $T_{a-max}$ , red line) for the annual (a),  
 771 warm (b), and cold (c) seasonal scales for the reference period from 1961 to 1990. We  
 772 used Eq (1) to simultaneously adjust for the effects of surface solar radiation ( $R_s$ ) and  
 773 precipitation ( $P$ ) on  $T_{s-max}/T_{a-max}$  and then analyzed the changes in the interannual  
 774 variation of  $T_{s-max}/T_{a-max}$  (section 3.3).  
 775



776

777 Figure 8. Maps of the trends of the monthly anomalies for the daily maximum land  
 778 surface temperature ( $T_{s-max}$ , a, c, e) and daily maximum air temperature ( $T_{a-max}$ , b, d, f)  
 779 for the annual, warm, and cold seasonal scales after adjusting for the effects of surface  
 780 solar radiation ( $R_s$ ) and precipitation ( $P$ ). We used Eq (1) to simultaneously adjust the  
 781 effects of  $R_s$  and  $P$  on  $T_{s-max}/T_{a-max}$  and then analyzed the changes in the secular trends  
 782 of  $T_{s-max}/T_{a-max}$  (section 3.3).



783

784 Figure 9. (a) Maps of the trends of surface solar radiation ( $R_s$ ) and the location of the  
 785 regions selected for further analysis: R1 (latitude: 30°–40° N; longitude: 110°–120° W)  
 786 and R2 (latitude: 30°–40° N; longitude: 100°–110° W). (b) National mean trends for  
 787 R1 and R2. (c) Annual, warm, and cold seasonal scale trends calculated based on the  
 788 data before adjustment. (d) Annual, warm, and cold seasonal scale trends calculated  
 789 based on the adjusted data (Wang et al., 2015a), which did not include the effect of the  
 790  $R_s$  variations. All error bars indicate the 95% confidence interval.

791

792 Table 1. Warming rates (unit: °C 10yr<sup>-1</sup>) of the temperatures ( $T_{s-max}$ ,  $T_{s-min}$ ,  $T_{a-max}$ ,  $T_{a-min}$ )  
793 for the annual, warm and cold seasonal scales. Raw and Adjusted represent the warming  
794 rates calculated for the data before and after adjusting for the effect of surface solar  
795 radiation ( $R_s$ ) and precipitation ( $P$ ), respectively. In Method I, the national mean  
796 anomalies were calculated first and then the national mean trend based on this time  
797 series was calculated. In Method II, the trend of each grid was calculated first and then  
798 the national mean value of the trends of all grids was calculated using the area-weight  
799 average method. We calculated the national mean trends of the temperatures using both  
800 methods.

			$T_{s-max}$	$T_{s-min}$	$T_{a-max}$	$T_{a-min}$
Method I	Raw	Annual	0.227±0.091	0.315±0.058	0.167±0.068	0.356±0.057
		Warm	0.172±0.103	0.221±0.054	0.091±0.056	0.245±0.049
		Cold	0.354±0.149	0.447±0.101	0.294±0.123	0.505±0.098
	Adjusted	Annual	0.373±0.068	-	0.222±0.062	-
		Warm	0.350±0.064	-	0.160±0.046	-
		Cold	0.450±0.119	-	0.329±0.114	-
Method II	Raw	Annual	0.254±0.197	0.328±0.094	0.183±0.103	0.368±0.082
		Warm	0.193±0.285	0.235±0.095	0.104±0.109	0.256±0.081
		Cold	0.321±0.267	0.415±0.159	0.264±0.167	0.476±0.139
	Adjusted	Annual	0.401±0.137	-	0.239±0.086	-
		Warm	0.374±0.173	-	0.174±0.082	-
		Cold	0.432±0.208	-	0.304±0.152	-
Units: °C 10yr <sup>-1</sup> . ±95% Confidence interval.						

801

802

